CrystEngComm

ROYAL SOCIETY OF CHEMISTRY

PAPER

View Article Online
View Journal | View Issue

Cite this: *CrystEngComm*, 2024, **26**, 4826

Theoretical investigation on enhanced HER electrocatalytic activities of SiC monolayers through nonmetal doping and strain engineering

Bingwen Li,†[a] Hongrui Shi,†[a] Zeyun Ni,†[a] Haifeng Zheng,†[c] Kehao Chen,†[a] Yuting Yan,[a] Huimin Qi,[a] Xue Yu,*[a] Xinfang Wang*[a] and Liming Fan *[b]

Received 22nd June 2024,
Accepted 6th August 2024

DOI: 10.1039/d4ce00633j

rsc.li/crystengcomm

Efficient hydrogen evolution reaction (HER) electrocatalysts are crucial for renewable energy storage and conversion. Pt remains the most efficient HER catalyst, but its widespread application is hindered by cost and resource constraints. In this study, we investigate the HER electrocatalytic activities of free-metal SiC monolayers through doping and strain engineering. Through density functional theory (DFT) calculations, we explore the effects of B, N, S, and P doping on the HER performance of SiC. Our results reveal that B and P doping enhance the catalytic activity, with P doping showing the most promising activity due to its smaller ΔG_{H^*} values. Furthermore, we apply tensile strain to modulate the HER activity of P-doped SiC, achieving further improvements. We also construct composite structures of P-doped SiC with graphene, enhancing conductivity and catalytic performance. Our findings provide valuable insights into tailoring the HER catalytic properties of SiC monolayers, offering a pathway towards sustainable hydrogen production.

Introduction

Renewable energy storage and conversion technologies are indispensable in combatting global environmental pollution and addressing the energy crisis.[1–6] Hydrogen, as an alternative energy carrier, offers numerous advantages such as high energy density, recyclability, and eco-friendly by-products.[7–9] Electrochemical water splitting has emerged as a sustainable, efficient, and environmentally benign method for large-scale hydrogen production, devoid of greenhouse gas emissions or other pollutants.[10–14] However, the hydrogen evolution reaction (HER), a crucial step in water-splitting, poses challenges requiring highly active catalysts to minimize overpotential effectively.

While noble-metal Pt remains the most efficient HER electrocatalyst, its widespread application in large-scale hydrogen generation is impeded by prohibitive costs and resource limitations.[15,16] To overcome this hurdle, extensive efforts have been dedicated to identifying non-precious and highly efficient HER catalysts as alternatives to Pt-based materials. Both experimental and theoretical investigations have highlighted promising prospects for various materials, including phosphides, sulfides, metal–organic complexes, carbon-based materials, *etc.*, to serve as HER electrocatalysts.[17–26]

Two-dimensional (2D) materials have attracted considerable interest in electrocatalysis due to their unique planar structure with atomic thickness, offering advantages such as large specific area and abundant active sites.[24,27,28] Graphene, a prominent member of the 2D material family, despite its inherent electrochemical inertness, has been the focus of efforts to enhance its catalytic performance in the HER through strategies like heteroatom doping and strain engineering.[29–31]

The 2D binary SiC, composed of C and Si atoms within the same main group as C, can be seen as an analogue of graphene. In 2009, Chu *et al.* reported that nanoscale 3C-SiC exhibited decomposing water molecules into –H and –OH. Ultra-thin 3C-SiC nanocrystals were later found to efficiently produce hydrogen under weakly acidic conditions.[32] Surface silicon atoms with dangling bonds displayed higher chemical activity, with Si–Si dimers being crucial in water decomposition. Theoretical simulations showed that surface-hydrogenated 3C-SiC nanoclusters followed a Heyrovsky–Volmer mechanism under acidic conditions.[33] Recently, Guo *et al.* created SiC-GD@GNRs composite structures, achieving an overpotential of only 63.5 mV at 10 mA cm^{-1} (ref. 2 and 34). Two-dimensional SiC monolayers doped with alkali and alkali earth metals show hydrogen evolution catalytic activity, with Be atom doped SiC exhibiting the best performance.[35]

[a] *Shandong Key Laboratory of Biophysics, Institute of Biophysics, College of Chemistry and Chemical Engineering, Dezhou University, Dezhou, 253023, P. R. China. E-mail: yuxuefish@163.com, dzwxf@126.com*
[b] *School of Chemistry and Chemical Engineering, North University of China, Taiyuan 030051, P. R. China. E-mail: limingfan@nuc.edu.cn*
[c] *Department of Physics and Electronic Information Engineering, Lyuliang University, No. 1 Xueyuan Road, Lishi District, Lyuliang 033000, Shanxi Province, China*
† These authors contributed equally to this work.

Meanwhile, Chen *et al.* reported that the similar two-dimensional GeSi, SnSi, and SnGe monolayers, which are structural analogues of the famous graphene, exhibit HER activity.[36–38]

In this study, we would like to investigate the HER electrocatalytic activities of SiC with nonmetal doping, and it is highly expected that they can exhibit good electrocatalytic performance. Furthermore, we also proposed effective ways through applying axial strain and construct composite structures with graphene to further improve their electrocatalytic activities.

Computational methods

The generalized gradient approximation of the Perdew–Burke–Ernzerhof functions of the studied systems within the frame of the Vienna *ab initio* simulation package (VASP).[39–41] A 4 × 4 supercell was used to guarantee the accuracy and efficiency of calculation results, and a vacuum region of 15 Å along the *z*-direction was set to avoid the spurious interactions between adjacent units. The kinetic energy cutoff was set to 450 eV and a semi-empirical van der Waals correlation (vdW) proposed by Grimme (DFT-D2) was used to account for the dispersion interactions.[42] In addition, the Monkhorst–Pack grid *k*-points of 5 × 5 × 1 were employed for the structural optimization.[43] The convergence criterion of energy and force in the calculations were set to 1.0×10^{-5} eV and 0.02 eV $Å^{-1}$, respectively. The *ab initio* molecular dynamics (AIMD) simulated at 300 K with DS-PAW software.[44]

The HER catalytic activity was estimated using the Gibbs free energy change (ΔG_{H^*}), which can be defined by the following equation:[45,46]

$$\Delta G_{H^*} = \Delta E_{H^*} + \Delta ZPE - T\Delta S_{H^*} \quad (1)$$

in which ΔE_{H^*} stands for the energy difference of hydrogen adsorption, and ΔZPE and ΔS denote the corresponding changes of zero point energy and entropy of H* adsorption, respectively. The qvasp code was used for postprocessing of the VASP computational data.[47]

Result and discussion

The structure, electronic properties and catalytic activities of SiC

The 2D SiC monolayer possesses a structure similar to graphene, we utilized a 4 × 4 SiC supercell structure as the initial model, and its geometric structure is shown in Fig. 1a. The lattice parameters is 12.376 Å, and the corresponding calculated bond lengths d_{Si-C}, are 1.786 Å, which are well consistent with the previously reported values. The band structure is shown in Fig. 1b and the band gap is 2.54 eV. Subsequently, we carried out the relevant calculations to estimate the HER catalytic activity of 2D SiC monolayer systems. It is well known that the HER catalytic activity of a material is closely correlated to the adsorption energy of a single H atom on its surface, so the adsorption Gibbs free energy of H* (ΔG_{H^*}) can be used as a reliable indicator to evaluate the HER catalytic activity of the site. Usually, a smaller absolute value of ΔG_{H^*} means better HER activity. Therefore, in this study the HER catalytic activities of the studied systems are also estimated by calculating the ΔG_{H^*} values. The detailed expression for calculating ΔG_{H^*} is given in the computational methods. Initially, we explore the HER catalytic activity of 2D SiC systems by calculating the ΔG_{H^*} values, where the top of Si and C adsorption sites are considered. The configurations with the adsorption of H* at the top sites of SiC monolayers can be obtained, as shown in Fig. 2a. Our computed results reveal that the corresponding ΔG_{H^*} values of the T_{Si} and T_C sites on the SiC monolayer are 1.360 and 1.623 eV, (Fig. 2b). Clearly, compared with the T_C site of graphene (1.858 eV), the ΔG_{H^*} values for the top sites (T_{Si} and T_C) are smaller.[38] This can be mainly attributed to the fact that the Si atoms have weaker π-bonding ability than the C atoms in the same main group, which is beneficial for the interaction of Si atoms with H* by adopting sp^3 hybridization when the HER takes place.

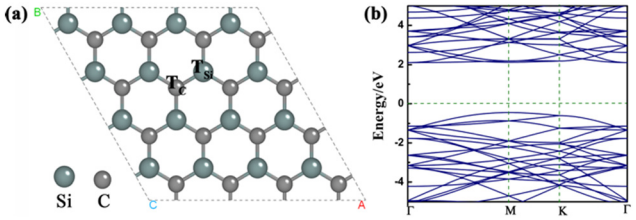

Fig. 1 (a) The optimized structures for the 2D SiC monolayer and (b) the band structure of the 2D SiC monolayer.

The structure, electronic properties and catalytic activities of X-SiC (X = B, N, P and S)

Based on the above discussions, we can understand that, compared with graphene, the 2D structural SiC can exhibit a better activity in catalyzing the HER process owing to the weaker aromaticity. However, their HER catalytic performances have to be further improved in view of the relatively large ΔG_{H^*} values. Here, we intend to enhance the HER catalytic activity of 2D SiC systems by doping atoms of B, N, P and S. It is highly

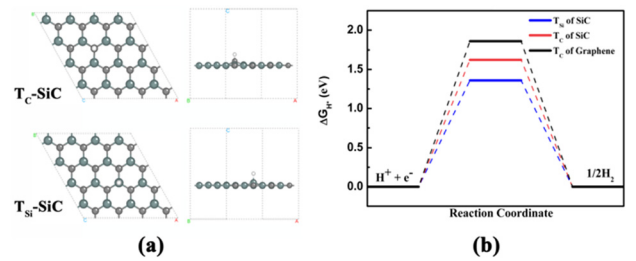

Fig. 2 (a) The optimized structures of H atoms adsorbed on the top of C and Si atoms of SiC. (b) The calculated free-energy diagram of the HER on the SiC structures for C and Si adsorption sites.

expected that high HER activity can be achieved in these doped SiC systems. Initially, we can obtain the doped structures for SiC by replacing the target C or Si atoms with B, N, P and S, respectively (Fig. 3). For convenience, these doped systems are denoted as $X_{C/Si}$-SiC, where X represents the dopant atom. In the B and N doped SiC structures, all atoms lie in the same plane, whereas, in the S and P-doped structures, the S and P atoms are not coplanar with SiC lattice, and the S and P atoms deviate significantly from the surface. The corresponding bond lengths of the doped atoms with the C/Si atoms are listed in Table 1. Moreover, we also explore the electronic properties of these doped SiC systems by calculating their band structures (Fig. 3). Our computed results reveal that B_{Si}-SiC and N_C-SiC systems exhibit metallic behavior, and the other systems also maintain semiconductor behavior. Compared with the pristine SiC, the band gap uniformly decreases significantly, especially the B_C-SiC, N_{Si}-SiC, P_C-SiC and P_{Si}-SiC systems, in which the band gaps are 0.35, 0.19, 0.40 and 0.60 eV, respectively (Fig. 3 and Table 1), which increases the conductivity. Their excellent conductivity is advantageous for the progress of the electrocatalytic HER process. Based on the optimized structures, the thermal stabilities of 2D monolayer systems are examined through performing AIMD simulations at 300 K with DS-PAW software. As shown in Fig. 4, the total energy can fluctuate near the equilibrium value and the structure can be well retained, confirming their good thermal stabilities.

Subsequently, we investigate the HER activities of these doped SiC systems by calculating the ΔG_{H^*} values of the adsorption sites. Ultimately, the configurations can be obtained with the adsorbed H* at the top sites over the dopant X or C/Si atoms, which are represented as T_X and T_C/T_{Si}, respectively, as illustrated in Fig. 5. The computed results revealed that the H atom can be stably adsorbed on the adsorption site of the top of doped atom X (X = N, S and P)

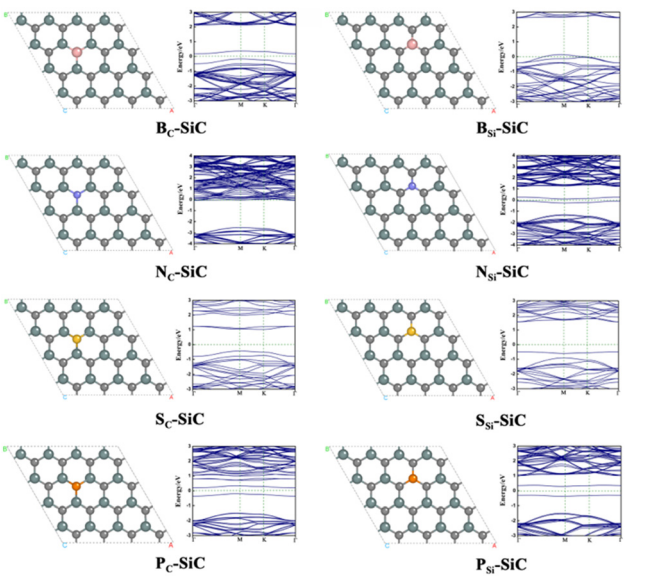

Fig. 3 The optimized structures and band structures for B, N, S and P doped C or Si atom in the SiC monolayer, respectively.

Table 1 The bond length $d_{X-C/Si}$ of doped atom X (X = B, N, S and P) with the C/Si atom in the SiC monolayer, the calculated band gaps of $X_{C/Si}$-SiC systems, and the computed ΔG_{H^*} (eV) values for H* at different adsorption sites (S_{ad}) on the $X_{C/Si}$-SiC systems

	$d_{X-C/Si}$ (Å)	Band gap (eV)	S_{ad}	ΔG_{H^*} (eV)
SiC	1.786	2.54	T_{Si}	1.35
			T_C	1.49
B_C-SiC	1.887	0.35	T_{Si}	—
			T_B	−0.92
B_{Si}-SiC	1.594	Metallic	T_B	—
			T_C	−0.82
N_C-SiC	1.775	Metallic	T_{Si}	−1.69
			T_N	1.98
N_{Si}-SiC	1.471	0.19	T_N	0.81
			T_C	0.56
S_C-SiC	2.307	1.46	T_{Si}	−0.01
			T_S	1.32
S_{Si}-SiC	1.798	2.06	T_S	2.54
			T_C	1.67
P_C-SiC	2.258	0.40	T_{Si}	0.77
			T_P	0.32
P_{Si}-SiC	1.767	0.60	T_P	−0.63
			T_C	0.57

and C/Si atom, respectively. For B atom doped C atom in the SiC monolayer (B_C-SiC), the H atom adsorption site is only the top of B atom, whereas the H atom adsorption site is only the top of C atom for the B atom doped Si atom (B_{Si}-SiC).

As revealed by the computed ΔG_{H^*} values (Fig. 6 and Table 1), doping B and P atoms uniformly improves the HER performance of the 2D SiC monolayer compared to doped N and S doped systems, resulting in considerably high HER activity. We first examine the effect of doping B on the HER catalytic activities of the 2D SiC systems. Our computed results reveal that when B substituted the C atom into SiC, the top adsorption site of doping B atom (T_B) is the main active site that exhibit a ΔG_{H^*} value of −0.92 eV, however, when B substituted the Si atom into SiC, the top adsorption site of C atom (T_C) doping sites is the main active site that exhibit a ΔG_{H^*} value of −0.82 eV. Obviously, doping B atoms can increase the HER catalytic activity of 2D SiC. For the N doped SiC systems, when N substituted the C atom into SiC, the top site of N and Si atoms has a ΔG_{H^*} value of −1.69 and 1.98 eV; however when N substituted the Si atom into SiC, the top site of N and C atoms has a ΔG_{H^*} value of −0.81 and 0.56 eV, respectively. So doping N atoms to substitute Si atoms exhibit a certain HER catalytic activity. When S substituted the Si atom into SiC systems, the catalytic activity of the HER on the top adsorption site of T_S and T_C is weak, where the ΔG_{H^*} values are 2.54 eV and 1.67 eV, respectively. However, when S substituted the C atom into SiC systems, the H atom adsorbed on the S atop exhibit a larger ΔG_{H^*} value of 1.32 eV, whereas the H atom adsorbed on the Si atop exhibit a ΔG_{H^*} value of nearly zero, which exhibits an excellent catalytic activity of the HER, but the S_C-SiC systems exhibit a large bandgap of 1.46 eV. So doping S atoms into SiC systems exhibits poor HER catalytic activity. For the P doped SiC systems, when P substituted the C atom into SiC,

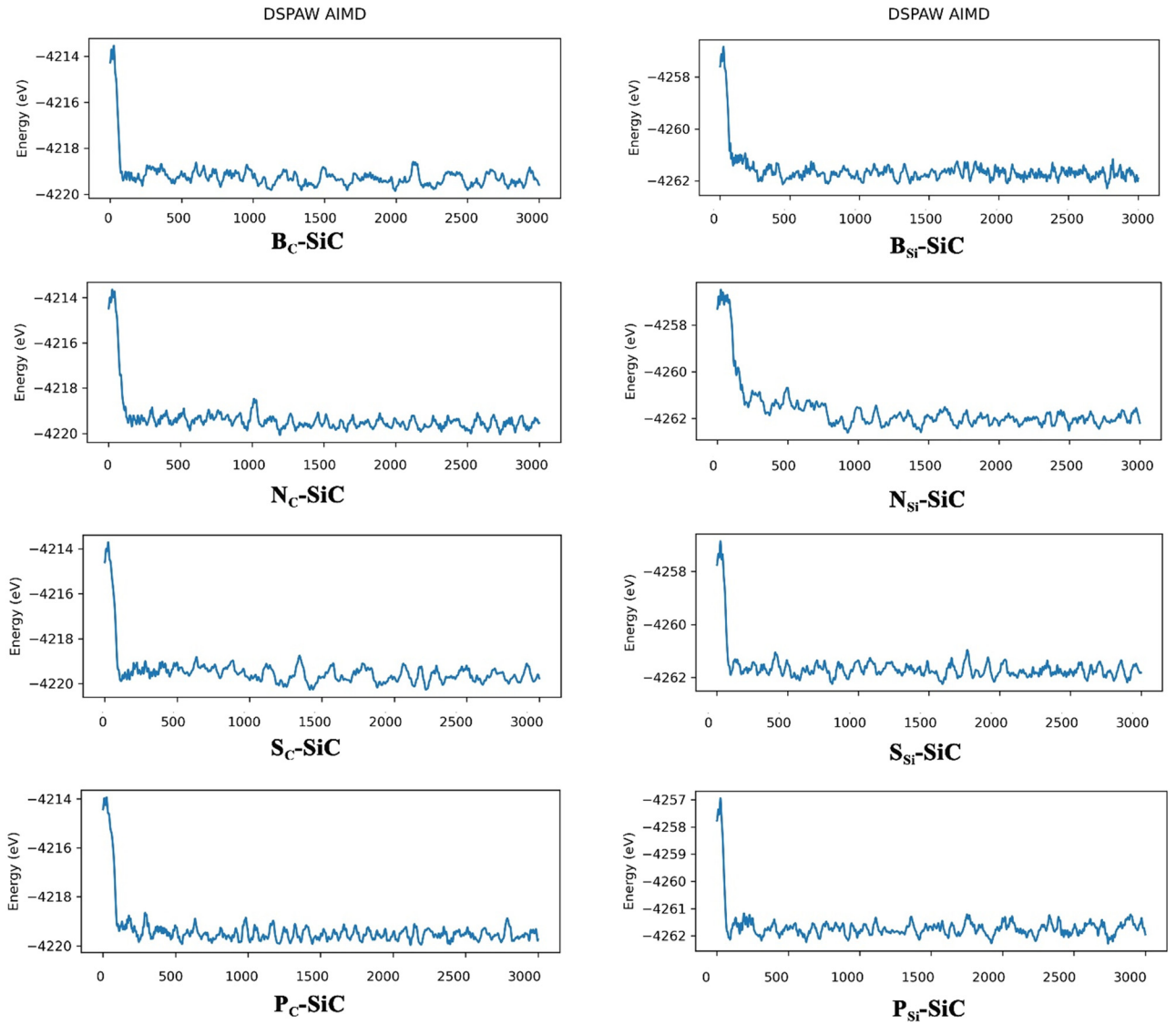

Fig. 4 Total energy curves of *ab initio* molecular dynamics (AIMD) simulation for $X_C/_{Si}$-SiC (X = B, N, S and P) systems at 300 K.

the top site of P and Si atoms has a ΔG_{H^*} value 0.77 and 0.32 eV; however when P substituted the Si atom into SiC, the top site of P and C atom has a ΔG_{H^*} value −0.63 and 0.57 eV, respectively, and the substituted P atoms exhibit a certain HER catalytic activity for SiC monolayer systems. Obviously, the HER performance of 2D SiC is effectively improved by doping B, N and P atoms, and the P atom is superior to the others, in view of the smaller ΔG_{H^*} value for the active sites.

Applying tensile strain to boost the HER catalytic activities of P_{Si}-SiC

Based on the above discussion, the P atom doped SiC system exhibit a small bandgap with good conductivity and smaller ΔG_{H^*} value, which is considered to be an excellent HER catalyst. In order to enhance the HER catalyst activity, we were applying tensile strain to modulate the HER activity. For the HER process, the H atom adsorbed on the active site is the first step, so we choose the H atom adsorbed on the top of the P atom in the P_{Si}-SiC as the study system, in which ΔG_{H^*} is negative that the H atom automatically adsorbs to the active site.

We calculated the ΔG_{H^*} values of P_{Si}-SiC under different tensile strains in the range of 0–10% (Fig. 6b). Under the condition of no tensile strain, the ΔG_{H^*} value of $(T_P)P_{Si}$-SiC is −0.63 eV while the ΔG_{H^*} values gradually increase with the increase of tensile strain from 0 to 10%, indicating considerably high HER activity. When the stress reaches 10%, the ΔG_{H^*} value is −0.46 eV, which is not comparable to the catalytic activity of the noble metal Pt. In addition, due to the band gap of P_{Si}-SiC systems, its weak conductivity will affect its HER catalytic activation. So we combined the P_{Si}-SiC structure with graphene (denoted as P_{Si}-SiC@G) and explored its HER catalytic activation. The structure of P_{Si}-SiC@G is shown in Fig. 7a and the computed results revealed that the band structure of P_{Si}-SiC@G is metallic, indicating that the composite system P_{Si}-SiC and graphene

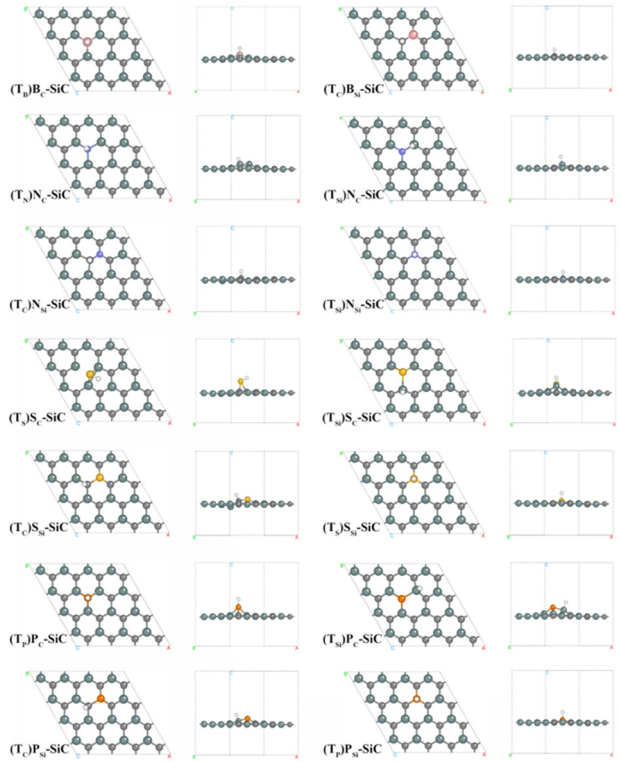

Fig. 5 The top and side views of optimized structures of the H atom at the top adsorption site of X (T_X) or C/Si (T_C/T_{Si}) atoms in the $X_{C/Si}$-SiC systems (X = B, N, S and P), respectively.

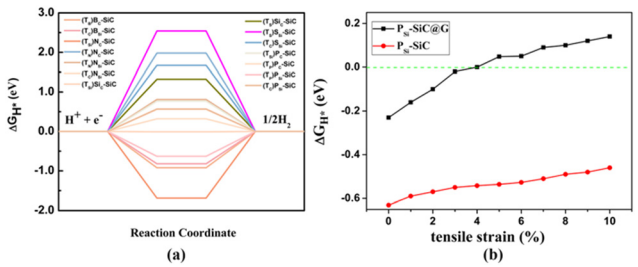

Fig. 6 (a) The computed ΔG_{H^*} values at the top sites of X-SiC systems (X = B, N, S and P) and (b) the computed ΔG_{H^*} values at the T_P sites as a function of tensile strain for P_{Si}-SiC and P_{Si}-SiC@G systems.

display excellent conductivity, which is conducive to HER catalytic activation. Moreover, the AIMD simulation of P_{Si}-SiC@G at 300 K was examined, and revealed that the total energy fluctuates near the equilibrium value in which the structure can be well retained, confirming their good thermal stabilities. Then we calculated the HER performance of P_{Si}-SiC@G; the ΔG_{H^*} value is −0.23 eV (Fig. 6b), which is obviously superior to the P_{Si}-SiC system. In order to further enhance the HER activity of P_{Si}-SiC@G systems, we applied tensile strain 0–10% on P_{Si}-SiC@G. As the tensile strain increases, the ΔG_{H^*} value gradually increases, and the P_{Si}-SiC@G monolayer exhibit the best HER catalytic activity with a ΔG_{H^*} value of −0.022 eV and 0.001 eV under 3% and 4% tensile strain, respectively (Fig. 6b).

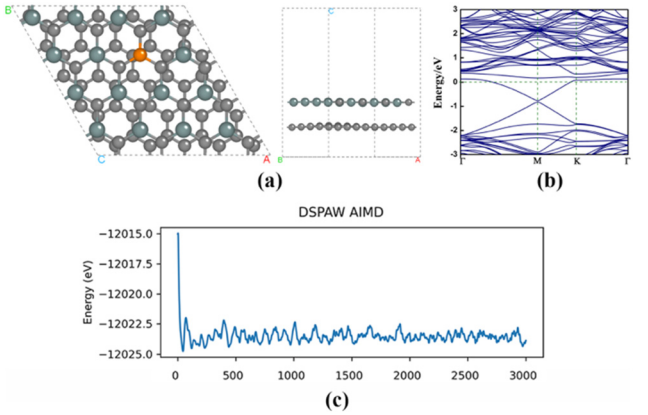

Fig. 7 (a) The optimized structure of P_{Si}-SiC@G, (b) the band structure of P_{Si}-SiC@G, and (c) the total energy curve of *ab initio* molecular dynamics (AIMD) simulation for the P_{Si}-SiC@G system at 300 K.

Overall, doping atoms (B, N, S and P) with different electronegativities can regulate the HER catalytic performance of the 2D SiC monolayer. Moreover, applying tensile strain and making a composite with graphene can effectively enhance the HER catalytic performance of the P atom doped 2D SiC system, and the catalytic performance can be comparable to Pt metal.

Conclusion

Our theoretical investigation sheds light on the enhanced HER electrocatalytic activities of SiC monolayers through nonmetal doping and strain engineering. By employing density functional theory calculations, we systematically studied the effects of B, N, S, and P doping on the HER performance of 2D SiC. Our results demonstrate that B and P doping notably improve the catalytic activity, with P doping exhibiting the most promising results due to its smaller ΔG_{H^*} value of −0.63 eV. Moreover, we found that applying tensile strain further enhances the HER activity of P_{Si}-SiC, offering additional improvements in catalytic performance. Additionally, we explored the composite structure of P_{Si}-SiC with graphene, which exhibited enhanced conductivity and catalytic activity; meanwhile, the tensile strain of 3% and 4% applied on thr P_{Si}-SiC@G system can exhibit excellent HER performance comparable to Pt metal. Our findings provide valuable insights into the design and development of efficient HER catalysts based on 2D SiC monolayers, offering promising prospects for sustainable hydrogen production and renewable energy technologies. Further experimental validation of these theoretical predictions would be essential for realizing their practical applications in the field of electrocatalysis.

Data availability

The data supporting this study's findings are available from the corresponding author upon reasonable request.

Author contributions

Bingwen Li: software, resources, project administration, writing – review & editing, and funding acquisition. Hongrui Shi: software, investigation, and writing. Zeyun Ni: investigation and software. Haifeng Zheng: formal analysis, validation, and visualization. Kehao Chen: investigation, software, and visualization. Yuting Yan: software. Huimin Qi: supervision. Xue Yu: conceptualization. Xinfang Wang: conceptualization. Liming Fan: conceptualization.

Conflicts of interest

The authors declare no competing financial interest.

Acknowledgements

This work is supported by the Natural Science Foundation of Shandong Province (ZR2021QB159). This work is also supported by the Talent Program Foundation of Dezhou University (NO. 2021xjrc102). We acknowledge the support from the Youth Innovation Team Lead-education Project of Shandong Educational Committee. We gratefully acknowledge the software support from HZWTECH. We thank Shenbo Yang and Yi Zhang (all from HZWTECH) for help and discussions regarding this study.

References

1 Z. P. Cano, D. Banham, S. Ye, A. Hintennach, J. Lu, M. Fowler and Z. Chen, *Nat. Energy*, 2018, **3**, 279–289.
2 J. Chow, R. J. Kopp and P. R. Portney, *Science*, 2003, **302**, 1528–1531.
3 Q. Xu, B. Qian, Y. Zhang, H. Li and Y. Wu, *ACS Appl. Energy Mater.*, 2022, **5**, 13562–13570.
4 S. Chu and A. Majumdar, *Nature*, 2012, **488**, 294–303.
5 C. W. Zheng, Q. Wang and C. Y. Li, *Renewable Sustainable Energy Rev.*, 2017, **79**, 1492–1502.
6 Y. Hu, J. Chen, Z. Wei, Q. He and Y. Zhao, *J. Mater. Inf.*, 2023, **3**, 18.
7 G. Gao, Y. Jiao, F. Ma, Y. Jiao, E. Waclawik and A. Du, *J. Phys. Chem. C*, 2015, **119**, 13124–13128.
8 T. He, P. Pachfule, H. Wu, Q. Xu and P. Chen, *Nat. Rev. Mater.*, 2016, **1**, 1–17.
9 J. A. Turner, *Science*, 2004, **305**, 972–974.
10 B. You and Y. Sun, *Acc. Chem. Res.*, 2018, **51**, 1571–1580.
11 X. Zou and Y. Zhang, *Chem. Soc. Rev.*, 2015, **44**, 5148–5180.
12 W. Liu, W. Liu, T. Hou, J. Ding, Z. Wang, R. Yin, X. San, L. Feng, J. Luo and X. Liu, *Nano Res.*, 2024, **17**, 4797–4806.
13 Z. Peng, Q. Zhang, G. Qi, H. Zhang, Q. Liu, G. Hu, J. Luo and X. Liu, *Chin. J. Struct. Chem.*, 2024, **43**, 100191.
14 W. Li, K. Liu, S. Feng, Y. Xiao, L. Zhang, J. Mao, Q. Liu, X. Liu, J. Luo and L. Han, *J. Colloid Interface Sci.*, 2024, **655**, 726–735.
15 Y. Zheng, Y. Jiao, M. Jaroniec and S. Z. Qiao, *Angew. Chem., Int. Ed.*, 2015, **54**, 52–65.
16 B. E. Conway and B. V. Tilak, *Electrochim. Acta*, 2002, **47**, 3571–3594.
17 R. Zhang, C. Tang, R. Kong, G. Du, A. M. Asiri, L. Chen and X. Sun, *Nanoscale*, 2017, **9**, 4793–4800.
18 Q. Xu, H. Li, Y. Shi, Z. Bi and Y. Wu, *ACS Appl. Nano Mater.*, 2021, **4**, 600–611.
19 J. Kibsgaard, Z. Chen, B. N. Reinecke and T. F. Jaramillo, *Nat. Mater.*, 2012, **11**, 963–969.
20 L. Zhang, Z. Yan, X. Chen, M. Yu, F. Liu, F. Cheng and J. Chen, *Chem. Commun.*, 2020, **56**, 2763–2766.
21 Y. Zhao, F. Zhao, X. Wang, C. Xu, Z. Zhang, G. Shi and L. Qu, *Angew. Chem., Int. Ed.*, 2014, **53**, 13934–13939.
22 H. Lin, Z. Shi, S. He, X. Yu, S. Wang, Q. Gao and Y. Tang, *Chem. Sci.*, 2016, **7**, 3399–3405.
23 Z. Zhou, L. Wei, Y. Wang, H. E. Karahan, Z. Chen, Y. Lei, X. Chen, S. Zhai, X. Liao and Y. Chen, *J. Mater. Chem. A*, 2017, **5**, 20390–20397.
24 X. Zhang, A. Chen, Z. Zhang, M. Jiao and Z. Zhou, *J. Mater. Chem. A*, 2018, **6**, 11446–11452.
25 Q. Gong, Y. Wang, Q. Hu, J. Zhou, R. Feng, P. N. Duchesne, P. Zhang, F. Chen, N. Han, Y. Li, C. Jin, Y. Li and S. T. Lee, *Nat. Commun.*, 2016, **7**, 13216.
26 J.-S. Qin, D.-Y. Du, W. Guan, X.-J. Bo, Y.-F. Li, L.-P. Guo, Z.-M. Su, Y.-Y. Wang, Y.-Q. Lan and H.-C. Zhou, *J. Am. Chem. Soc.*, 2015, **137**, 7169–7177.
27 J. Liu, G. Yu, X. Huang and W. Chen, *2D Mater.*, 2019, **7**, 015015.
28 X. Liu, G. Li, J. Liu and J. Zhao, *Mol. Catal.*, 2022, **531**, 112706.
29 S. Chandrasekaran, D. Ma, Y. Ge, L. Deng, C. Bowen, J. Roscow, Y. Zhang, Z. Lin, R. D. K. Misra, J. Li, P. Zhang and H. Zhang, *Nano Energy*, 2020, **77**, 105080.
30 B. You, M. T. Tang, C. Tsai, F. Abild-Pedersen, X. Zheng and H. Li, *Adv. Mater.*, 2019, **31**, e1807001.
31 R. Gusmão, M. Veselý and Z. Sofer, *ACS Catal.*, 2020, **10**, 9634–9648.
32 C. He, X. Wu, J. Shen and P. K. Chu, *Nano Lett.*, 2012, **12**, 1545–1548.
33 X. Shen and S. T. Pantelides, *J. Phys. Chem. Lett.*, 2013, **4**, 100–104.
34 X. Fan, Z. Peng, J. Wang, R. Ye, H. Zhou and X. Guo, *Adv. Funct. Mater.*, 2016, **26**, 3621–3629.
35 R. J. Baierle, C. J. Rupp and J. Anversa, *Appl. Surf. Sci.*, 2018, **435**, 338–345.
36 W. Liao, G. Yu, L. Zhao, H. Zhu and W. Chen, *Nanoscale*, 2022, **14**, 10918–10928.
37 Q. Wang, E. Yang, R. Liu, M. Lv, W. Zhang, G. Yu and W. Chen, *Molecules*, 2022, 28.
38 C. Li, G. Yu, X. Shen, Y. Li and W. Chen, *Molecules*, 2022, **27**, 5092.
39 G. Kresse and J. Furthmüller, *Comput. Mater. Sci.*, 1996, **6**, 15–50.
40 G. Kresse and J. Furthmuller, *Phys. Rev. B: Condens. Matter Mater. Phys.*, 1996, **54**, 11169–11186.

41 G. Kresse and D. Joubert, *Phys. Rev. B: Condens. Matter Mater. Phys.*, 1999, **59**, 1758–1775.
42 S. Grimme, *J. Comput. Chem.*, 2006, **27**, 1787–1799.
43 H. J. Monkhorst and J. D. Pack, *Phys. Rev. B: Solid State*, 1976, **13**, 5188–5192.
44 P. E. Blochl, *Phys. Rev. B: Condens. Matter Mater. Phys.*, 1994, **50**, 17953–17979.
45 J. Rossmeisl, A. Logadottir and J. K. Nørskov, *Chem. Phys.*, 2005, **319**, 178–184.
46 J. K. Nørskov, J. Rossmeisl, A. Logadottir, L. Lindqvist, J. R. Kitchin, T. Bligaard and H. Jónsson, *J. Phys. Chem. B*, 2004, **108**, 17886–17892.
47 W. Yi, G. Tang, X. Chen, B. Yang and X. Liu, *Comput. Phys. Commun.*, 2020, 257.